

Korali: a High-Performance Computing Framework for Stochastic Optimization and Bayesian Uncertainty Quantification

Sergio M. Martin, Daniel Wälchli, Georgios Arampatzis, Petros Koumoutsakos*

Computational Science and Engineering Laboratory, Clausiusstrasse 33, ETH Zürich, CH-8092, Switzerland

Abstract

We present a modular, open-source, high-performance computing framework for data-driven Bayesian uncertainty quantification and stochastic optimization. The proposed framework (Korali) is well suited for the non-intrusive sampling of computationally demanding engineering and scientific models. The framework's distributed-execution engine allows for the efficient execution of massively-parallel computational models while providing fault tolerance and load balancing mechanisms. In this paper, we present our framework's design principles and explain its flexibility in allowing scientists to deploy stochastic methods at scale. We demonstrate the capabilities of Korali for Bayesian inference and optimization studies using existing high-performance software such as LAMMPS (CPU-Based) and MIRHEO (GPU-Based) and show scaling efficiently on up to 4096 nodes of the CSCS Piz Daint supercomputer.

Keywords: High-Performance Computing, Uncertainty Quantification, Stochastic Optimization, Bayesian Inference

1. Introduction

Over the last thirty years, High-Performance Computing (HPC) architectures have enabled high-resolution simulations of physical systems ranging from molecules to galaxies. HPC has also reduced the cost and turnaround time of such simulations, making them invaluable predictive and design tools across all fields of science and engineering. Today, multiple simulations at resolutions that would have been impossible a decade ago are routinely employed in optimization and design.

More recently, HPC has become central in the new ways that we conduct science with massive amounts of data. Such data can be used to develop and calibrate physical models as well as to quantify the uncertainties of their predictions. The integration of data and physical models has a history of over 300 years, dating back to Laplace and Copernicus and to the framework known as Bayesian inference. However, due to its computational cost, the application of Bayesian inference has been, until recently, limited to simple models evaluated analytically or through inexpensive approximations. Bayesian inference requires the sampling of spaces with a dimensionality greater or equal to the number of model parameters, thus making it computationally demanding, particularly when the underlying model may require hundreds of CPU core-hours for a single realization. Moreover, special care is necessary to develop sampling algorithms¹ that harness the capabilities of modern supercomputers [1].

The need for efficient deployment of stochastic optimization and uncertainty quantification algorithms has not been overlooked, and several statistical frameworks have been developed for enabling stochastic optimization and Bayesian UQ of computational models [2, 3, 4, 5, 6, 7]. However, only a few such frameworks are well-suited for the deployment of such algorithms in massively parallel computer architectures [8, 9, 10]. In this paper, we present Korali, a new HPC framework for stochastic optimization and Bayesian inference. Korali's parallel execution engine provides efficient sampling on supercomputing platforms while introducing novel mechanisms for fault-tolerance, workload balancing, and reproducibility, essential requirements for the future Exascale supercomputers [11]. Our framework's design is modular, allowing the development and integration of new statistical methods and solvers to take advantage of its distributed execution engine. Lastly, code portability is enabled by a language-independent interface that allows users to run a variety of computational models in C++, Python, as well as pre-compiled applications.

The development of Korali was motivated by scientific studies that necessitate the data-driven inference of model parameters in large scale simulations [12, 13, 14]. In this work, we provide a performance analysis of our experiences testing our framework's novel features running on up to 4096 nodes, 71% of the CSCS *Piz Daint* supercomputer.

The rest of this paper is organized as follows: in Section 2, we explain the rationale of our framework; in Section 2.2, we describe the its user interface; in Section 3, we detail the implementation of our sampling engine; in Section 4, we present our results and analysis for three experimental cases; in Section 5, we discuss the state of the art of current UQ frameworks, and; in Section 6, we present conclusions and future work.

*Corresponding author

Email address: petros@ethz.edu (Petros Koumoutsakos)

¹We note that both stochastic optimization and Bayesian uncertainty quantification (UQ) algorithms are non-intrusive as they primarily rely only on an input/output relationship with the sampled model.

2. Framework Design

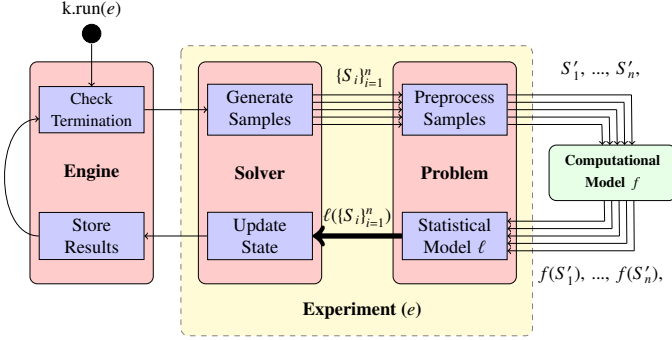


Figure 1: Generation-based workflow of the execution engine.

Korali’s framework is specifically tailored for the execution of population-based statistical algorithms such as Covariance Matrix Adaption Evolution Strategy (CMA-ES) [15] and Transitional Markov Chain Monte Carlo (TMCMC) [16]. These algorithms rely on generating sets of parameters (samples) iteratively. At each iteration, a set of n samples S_i are evaluated by a statistical model ℓ which, in turn, may require the execution of a computational model f representing, e.g., a complex physical simulation. The statistical model is given by choice of *problem*, which may be *Optimization*, to search the optimum (minimum or maximum) of an objective function; *Bayesian Inference* to sample the posterior distribution of a statistical model given some reference data, or; any of the other problem type families.

In order to deploy our framework, users define an *Experiment* (see Fig. 1). This *Experiment* specifies all the information required to define the problem, the solver algorithm, and the experiment’s *parameter space*. The parameter space represents the range of values within which the solution is to be identified, and it is determined by *variables*, which represent the inputs to the statistical and computational models. Variables are uniquely identified by their name and can be restricted through an upper and a lower bound, or described by a prior distribution. Prior distributions are also identified by name, and their properties can be defined by the user.

Once the problem, solver, and parameter space are fully defined, the user can start the experiment’s execution by running the execution engine (discussed in Section 3). The engine will coordinate the exchange of samples between the experiment’s modules, the statistical model, and the computational model until the solver terminates.

2.1. Generation-Based Sampling

Fig. 1 shows the workflow of the engine when executing a given experiment. A *generation* represents a cycle in which the experiment produces and evaluates a population of samples. We define a *sample* S_i as a particular selection of values for each of the experiment’s variables within the feasible parameter space, as defined by the variables’ prior distribution or lower/upper bounds.

The first generation starts when the application executes $k.run(e)$, where e is the user-defined experiment object and k represents an instance of the engine. The first step in every generation is to check whether any of the defined termination criteria has been met, in which case the execution returns to the user application. Otherwise, the engine yields execution to the solver method. The solver method generates an initial population of samples $\{S_i\}_{i=1}^n$ and relays them to the problem module for pre-processing. This module stores any statistical parameters from the sample and performs any required transformations on the computational parameters. The pre-processed samples (S'_i) are then relayed to the computational model, to evaluate each of them $\{f(S'_i)\}_{i=1}^n$.

After receiving the results from the computational model, the problem module calculates a derived quantity, e.g., the log-likelihood $\ell(S)$ for a problem of type Bayesian inference, also based on its reference data, and passes it back to the solver module. The derived quantities are standardized such that it can be used by any compatible solver method. Before the generation finishes, the solver updates its internal state and produces partial results, which serve as the basis for setting up the next generation, until a user-defined termination criterion is met.

2.2. Interface Design

One of the main challenges in developing a statistical analysis framework lies in designing an intuitive interface to describe the properties of an experiment and its coupling with external computational models. To address this challenge, Korali employs a fully *descriptive* interface, in which problems are defined from the statistician’s perspective using statistical nomenclature. This interface is mostly language-independent and requires only trivial knowledge of the underlying programming language (e.g., Python or C++).

Figure 2 shows an example of a Python-based² application that solves the problem of calibrating the parameters of a computational model on experimental data. We configured the example to describe a Bayesian inference problem where the uncertainty in the parameters is quantified by sampling the posterior distribution of the parameters conditioned on the data. To better explain the software interface, we define the statistical problem first, and then show its correspondence with the code in Fig. 2.

The output of the computational model that fits the experimental observations is a function f that depends on a vector of parameters $\boldsymbol{\theta}$ and a vector of input parameters \mathbf{x} with known values. Each observation y_i corresponds to a known input parameter \mathbf{x}_i for $i = 1, \dots, N$. We assume that each observation y_i is linked to the computational model through an *error equation*. Here, we assume that

$$y_i = f(\mathbf{x}_i; \boldsymbol{\theta}) + \varepsilon_i, \quad (1)$$

and ε_i are independent normal random variables with mean 0 and standard deviation $g(\mathbf{x}_i; \boldsymbol{\theta})$, where g is a positive function.

²Although we use Python in our examples, Korali provides a similar C++-based interface that allows linking its engine against C++ and Fortran computational models.

```

1  import korali
2
3  # Importing the computational model and the data
4  from myLibrary import F
5
6  X = getReferenceInput()
7  Y = getReferenceData()
8
9  # Creating new experiment
10 e = korali.Experiment()
11
12 # Setting up the Bayesian Inference Problem
13 e["Problem"]["Type"] = "Bayesian Inference"
14 e["Problem"]["Likelihood Model"] = "Normal"
15 e["Problem"]["Computational Model"] = lambda s: F(s,X)
16 e["Problem"]["Reference Data"] = Y
17
18 # Configuring the problem's variables and their priors
19 e["Variables"][0]["Name"] = "P1"
20 e["Variables"][1]["Name"] = "P2"
21 e["Variables"][2]["Name"] = "Sigma"
22 e["Variables"][0]["Prior Distribution"] = "D1"
23 e["Variables"][1]["Prior Distribution"] = "D1"
24 e["Variables"][2]["Prior Distribution"] = "D2"
25
26 # Configuring the prior distributions
27 e["Distributions"][0]["Name"] = "D1"
28 e["Distributions"][0]["Type"] = "Univariate/Normal"
29 e["Distributions"][0]["Mean"] = 0.0
30 e["Distributions"][0]["Sigma"] = +2.0
31
32 e["Distributions"][1]["Name"] = "D2"
33 e["Distributions"][1]["Type"] = "Univariate/Uniform"
34 e["Distributions"][1]["Minimum"] = 0.0
35 e["Distributions"][1]["Maximum"] = +5.0
36
37 # Configuring Solver (TMCMC) parameters
38 e["Solver"]["Type"] = "TMCMC"
39 e["Solver"]["Population Size"] = 5000
40 e["Solver"]["Covariance Scaling Factor"] = 0.04
41
42 # Starting Korali's Engine and running experiment
43 k = korali.Engine()
44
45 k.run(e)

```

Figure 2: Example of a Python-based Korali Application.

Using Bayes' theorem, our goal is to draw samples from the distribution

$$p(\boldsymbol{\theta}|\mathbf{y}; \vec{\mathbf{x}}) \propto p(\mathbf{y}|\boldsymbol{\theta}; \vec{\mathbf{x}}) p(\boldsymbol{\theta}), \quad (2)$$

where \mathbf{y} and $\vec{\mathbf{x}}$ are the variables that contain all the observations and all the input parameters, respectively. Under the assumption of Eq. (1), the likelihood function $p(\mathbf{y}|\boldsymbol{\theta}, \vec{\mathbf{x}})$ is given as a product of normal distributions. The density $p(\boldsymbol{\theta})$ is the prior distribution that encompasses all known information for the parameters $\boldsymbol{\theta}$ prior to observing any data.

The variables $\vec{\mathbf{x}}$ and \mathbf{y} correspond to the variables X and Y in the code of Fig. 2 that are initialized in Lines 6 and 7 through user defined functions. Korali works by defining and running an *experiment* (Line 10)³. An experiment consists of the description of a statistical problem to be solved, a description of the involved variables and their distributions, and the configuration of the desired solver to solve the problem with. In this application, all lines of code between Line 13 and Line 40 that are required for the description of the problem, are made entirely by specifying the problem type, the variables and their

prior distributions, and the solver method to be employed, via dictionary-tree accesses. The rest of the code consists of importing libraries (Lines 1 and 4), initializing the experiment (Line 10), initializing the engine (Line 43), and running Korali (Line 45).

The type of the problem is defined in Line 13, and the statistical model is defined in Line 14. The observations Y are passed to Korali in Line 16 and the computational model in Line 15. Notice that the computational model is assigned as a lambda function in order to pass the input parameters X directly to the computational model F . In top of Fig. 3 an example of a computational models are given, where $f(\mathbf{x}_i; \boldsymbol{\theta}) = \theta_1 x_i + \theta_2$ and $f(\mathbf{x}_i; \boldsymbol{\theta}) = \theta_3$.

Next, the parameter vector $\boldsymbol{\theta}$ is defined by the experiment's *variables*. Each variable is defined by a unique name and represents one entry to the parameter vector. The example code contains three variables, P1, P2 and Sigma, in Lines 19 to 21, respectively. The variables are passed in the user-defined model F and used to compute the functions f and g of Eq. (1), given by the keywords *Reference Evaluation* and *Standard Deviation*, respectively.

To complete the description of the problem, the variables require the definition of a prior distribution $p(\boldsymbol{\theta})$ by referencing the appropriate distribution by name. Here, we specify that the prior distribution of the variables corresponding to the parameters P1 and P2 is a normal distribution (Lines 22 and 23), and of the variable corresponding to the parameter Sigma a uniform distribution (Line 24). Finally, we set the solver to the TMCMC sampler [17]. The solver samples the posterior distribution through repeated computational model evaluations of the samples.

2.3. Computational Model Support

The user specifies the computational model by passing a function as part of the problem configuration. Such a function should expect a sample as a single argument. In the example in Fig. 2, the computational model is passed as a lambda function that calls the computational model F , imported from the *myLibrary* module.

Functions passed as computational models do not return a value. Instead, they save their results into the sample container. The expected results from the execution of the computational model depend on the selected problem type. Figure 3 (Top) shows the function F , as specified in the example in Fig. 2. A Bayesian inference problem, where the likelihood is computed from reference data, requires that the model saves an evaluation of each of the reference data points into a "Results" vector. Other problem types, such as *derivative-free optimization*, require the model to store only a single numerical value corresponding to the function evaluation (" $F(\mathbf{x})$ ") for the given parameter(s), as shown in Fig. 3 (Middle).

Our interface accommodates legacy codes through an External execution mode that allows instanting pre-compiled applications via shell commands and returns the results either through file or pipe I/O operations. The External mode can also be used to launch and gather results from large-scale dis-

³Note that experiments need not be stand-alone scripts, but can also be easily integrated as part of larger applications.

```

1 def F(sample, X):
2     p1 = sample["Variables"]["P1"]
3     p2 = sample["Variables"]["P2"]
4     s = sample["Variables"]["Sigma"]
5
6     s["Reference Evaluations"] = []
7     s["Standard Deviation"] = []
8     for x in X:
9         s["Reference Evaluations"] += [a*x + b]
10        s["Standard Deviation"] += [sig]
11
12 def myOptimizableModel(sample):
13     x = sample["Variables"]["X"]
14     sample["F(x)"] = -x * x
15
16 def myExternalModel(sample):
17     x = sample["Variables"]["X"]
18     args = [ './myApp', '-x', str(x) ]
19     result = subprocess.check_output(args)
20     sample["F(x)"] = float(result)

```

Figure 3: Examples of computational models. (Top): A model that has two parameters P1 and P2 and produces as result a vector of evaluations, one for each value of the input vector X. (Middle): A model that requires a single parameter X and produces a single function evaluation $f(x) = -x^2$, to be maximized using a derivative-free method. (Bottom): A model that executes an external application and returns its output as result.

tributed, *e.g.*, MPI [18] or UPC++ [19], applications. An example of such a model is given in Fig. 3 (Bottom). Although the External conduit provides flexibility in the execution of any computational model, it does require that the user specifies how the values from a sample will be extracted and passed to the model, as well as parsing the results from file or standard output.

2.4. Termination and Results

Every solver exposes a set of *Termination Criteria* which determine the conditions under which the execution terminates. Some criteria are active by default, such that the experiment provides a baseline guarantee of termination. In addition, some criteria are common to all solvers, such as the maximum number of computational model evaluations. After detecting that at least one termination criterion was met, the engine returns execution to the calling application and exposes the results via the experiment's interface. To access the results, a user can, for example, access the found optimum of an optimization problem via `e["Results"]["BestSample"]`, or the sampling output of a Bayesian inference problem via `e["Results"]["Sample Database"]`. These values are exposed as list of float values or dict data types.

After every generation, the engine also gathers all of the solver's state variables, including the results, and exports them to per-generation result files. Result files serve three purposes: (i) keep a record of all (intermediate) results produced during execution, (ii) store the execution state of the solvers to facilitate restarting in case of failure (see Section 3.3), and (iii) serve as input to plotting tools, which provide graphical analyses of the execution of the experiment and its results.

3. Parallel Execution Engine Design

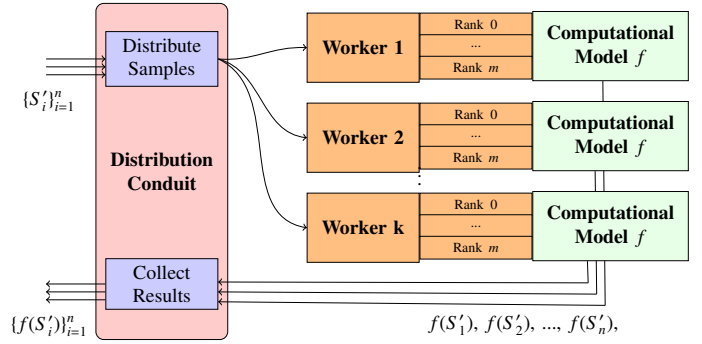


Figure 4: Distribution conduit for parallel models assigns samples to every worker and collects their results.

Although the software allows for the analysis of statistical problems that involve simple computational models (*i.e.*, those which can be quickly run in a consumer laptop), its execution engine is specifically tailored to support the execution of extreme-demanding computational models (*i.e.*, those running on thousands of supercomputer nodes). To enable parallel sample evaluation, the user runs multiple instances of the python script or C++ binary, typically via the `mpiexec` command⁴. The engine determines the number k of processes that have been instantiated and assigns roles to them. The first process assumes the role of the *'engine'*, managing sample production and evaluation, as shown in Fig. 1. The rest of $k - 1$ processes assume the role of *'workers'*, whose only task is to wait for incoming samples, run the computational model f , and to return their results.

The simultaneous distribution of samples and the collection of their results, is performed through a *distribution conduit* module between the experiment and the computational model. This conduit keeps track of the state of each worker (*i.e.*, *idle*, *working*, *pending*), and assigns any incoming samples workers that are currently in the *idle* state. As soon as a sample is received, a worker transitions to *busy* state, during which it executes f on the sample parameters. When the worker finishes executing f , it returns the results and sets its state to *pending*, indicating that the engine can collect the result. It is only after the execution conduit detects the pending results and retrieves them, that the worker state transitions back to *idle* again, signaling its availability to evaluate the next sample.

To handle sample distribution, some libraries, such as $\Pi 4U$ [8], use a *divide-and-conquer* strategy, in which they assign a fairly-split batch of samples to all workers at the beginning of each generation. Albeit simple, this approach is susceptible to load imbalance issues, by which some workers may require more time to finish due to variations in the samples' running time. To alleviate this effect, $\Pi 4U$, employs a job-stealing technique in which workers can steal samples from others during

⁴For systems that do not support MPI, the External execution mode can be used to run with multiple concurrent processes using a `fork/join` strategy instead.

runtime. This technique, however, requires complex coordination and constant communication between the workers and the engine. Korali avoids the problem of uneven sample distribution altogether by employing an *opportunistic* strategy in which the distribution conduit maintains a common queue of pending samples from which all workers are served. The conduit distributes samples on a one-by-one basis, in real-time, as soon as a worker becomes idle. This approach enforces that workers can hold at most one sample at any given time. Consequently, no single worker may keep more samples than another, thus eliminating the need for job stealing.

The format and size of the sample input parameters and results may vary depending on the problem type. For instance, some problem types expect a single floating-point number as the result of a sample evaluation, while others (e.g., gradient-based optimization) also require a vector of real numbers containing the function gradient for the given parameters. Such data heterogeneity is handled through the JSON [20] data interchange format to convert the evaluation results into a string that can be communicated back and forth between the conduit and workers. The distribution conduit uses MPI as backend communication layer, sending a single message per JSON-serialized sample and its results. With this approach, the conduit allows the distributed execution of any computational model, free from format restrictions on input and output data.

3.1. Support for Parallel Models

To support the execution of MPI-based computational models, the execution conduit creates a set of *worker teams*, each assigned a subset of MPI ranks, as illustrated in Fig. 4. All ranks belonging to the same team, work together in parallel to evaluate incoming samples. Users define the number of MPI ranks per team through the "Ranks Per Worker Team" configuration parameter (m). For an execution encompassing N MPI ranks (as specified in the `mpiexec` or similar launch command), one of which will be reserved as the execution engine, the conduit will create and manage k worker teams, as given by the formula:

$$k = \frac{N - 1}{m} . \quad (3)$$

Every worker team owns their private MPI communicator, which allows message passing between the ranks contained therein. Any MPI-based computational model passed to Korali should use this team-specific communicator for communication operations, instead of the generic `MPI_COMM_WORLD` communicator, which encompasses the entire MPI rank population. In this way, each sample evaluation will only use the number and identity of ranks allocated by the team to which it has been assigned.

Fig. 5 shows an MPI-based computational model. As previously described, the model is a function that receives a single sample as its parameter. In the case of parallel sampling, however, the conduit also appends an `MPI Communicator` field to the sample containing the communicator number that corresponds to the receiving worker team. With this value, the model can determine the m number of ranks in the team and the rank

```

1 def myMPIModel(sample):
2     comm = sample["MPI Communicator"]
3     rank = comm.Get_rank()
4     size = comm.Get_size()
5
6     x = sample["Variables"]["X"]
7     q = computeAndCommunicate(x, comm)
8
9     sample["F(x)"] = comm.Reduce(q)

```

Figure 5: Example of an MPI-based computational model that takes as input a single parameter from the sample and produces a result that requires both computation and communication operations among the team ranks.

identifiers therein. The model can then compute and communicate like a normal MPI application and produce a result collaboratively. After evaluation, only the results reported by rank 0 in the team are collected.

3.2. Multi-Experiment Support

The software allows the simultaneous execution of multiple independent experiments to increase the pool of pending samples at any given moment. This approach maximizes the occupation of workers, and increases the overall efficiency (see Section 4.2 for further discussion and a study case).

Fig. 6 shows a flow diagram of the framework when executing two experiments simultaneously (e_0 , and e_1) on a super-computer cluster. The execution engine switches its execution context between both experiments, constantly polling whether either is ready to advance to the next generation or return partial results for storage. During execution, each experiment produces and evaluates its own set of samples (S' , for e_0 , and; T' , for e_1).

The distribution conduit handles each experiment's samples independently, distributing them among the common set of workers. Depending on which experiment has issued the sample, the distribution conduit assigns the respective computational model function to run. In this case, f , if the sample belongs to e_0 , or; g , if the sample belongs to e_1 . The results are asynchronously returned to the collection module, which distributes them back to the corresponding experiment. The engine evaluates each experiment's termination criteria after the given experiment reaches the end of its current generation. It is only after all experiments have finished that execution is returned to the user's application. The results from each experiment are stored separately as if they had executed in different instances.

3.3. Modularity and Fault-Tolerance

The user community may extend Korali by adding new problem types and solver algorithms. To support extensibility, the software detects, during build-time, any new user-defined modules and integrates them into the pool of usable modules automatically. New modules will benefit from the parallel sampling engine without additional efforts. Such design represents a novelty among statistical frameworks, allowing scientists to test new methods for large-scale execution without the need to develop a tailor-made parallel sampling engine for each one.

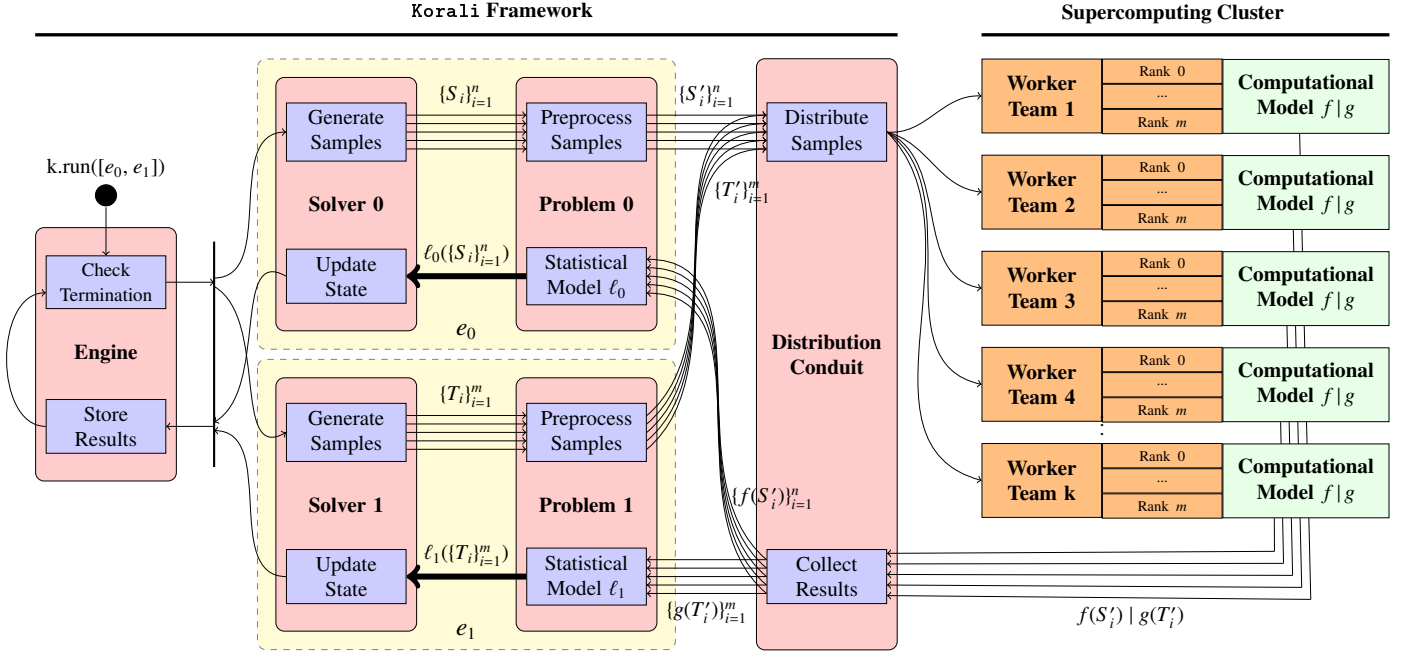


Figure 6: Dataflow diagram of Korali's execution engine.

```

1  # Creating Experiment List
2  eList = []
3
4  for i in range(N)
5      # Instantiating Experiment
6      e = korali.Experiment()
7
8      # Configuring experiment
9      ...
10
11     # Adding Experiment to the list
12     eList.append(e)
13
14     # Starting Korali's Engine and running experiment list
15     k = korali.Engine()
16     k.run(eList)

```

Figure 7: Example of a Python-based Application that runs N multiple experiments simultaneously.

To integrate a new module, developers add a new folder to the source, containing three source files with a well-defined format: their base C++ class declaration header file (.hpp), their base C++ class method definitions file (module.cpp), and their configuration file (.config). The software enforces that the base header declares the module class, allowing no class attribute declarations. Instead, attributes should be inserted as entries in the .config file. Each entry in the configuration file specifies a setting name⁵, its C++ data type, a full description of its purpose, and a default value.

The software ensures that all modules save their full internal state at the end of every generation onto a state file in the results

⁵These names are defined in a verbose, human-readable format which may include multiple space-separated words, which are later converted to a C++ compatible symbol, e.g., parameter "Sample Population" converts to a variable called `_samplePopulation`.

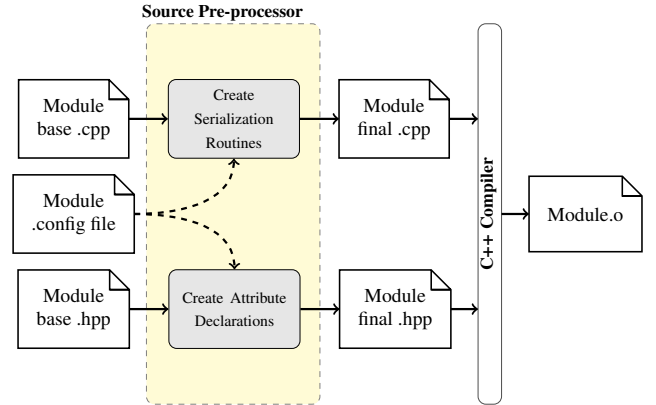


Figure 8: Automatic generation of serialization and de-serialization routines for Korali modules.

folder. The state file, which also contains the partial results of the execution, can serve as a checkpoint from which the execution can be resumed at a later stage, in case of failure or work splitting into shorter jobs. To relieve module developers from the effort and bug-prone process of developing these restart capabilities by hand, Korali provides a systematic way to create these routines automatically. Before compilation, based on the settings declared in the .config file, the base C++ header file is pre-processed to automatically add their corresponding declarations as class fields, as shown in Fig. 8. Serialization and de-serialization methods are then automatically created in the module class that saves and loads all its attributes to and from a JSON file, respectively. These methods are automatically called after each generation to create a new checkpoint. User-defined method definitions in the .cpp file can make use of

auto-generated attributes as if they were originally described in the class header. A secondary product of code pre-processing is the automatic production of documentation pages for all modules. Based on the contents of `.config` file, the pre-processor produces *reStructuredText Markup* (`.rst`) [21] files, containing human-readable entries that are automatically uploaded to the user manual [22].

At the end of every generation, the engine stores the internal state of any solver, including its random number generators. This procedure guarantees that in case of resuming an experiment from a file, both the evolution of the experiment and its partial results remain exactly as before.

4. Experimental Evaluation

To test the capabilities of Korali for extreme-scale efficiency and resilience, we ran three Bayesian inference experiments, motivated by previously proposed ideas from research. In our first experiment, we infer the parameters of a red blood cell (RBC) stretching experiment and demonstrate that Korali can achieve a high sampling efficiency on a large portion of modern supercomputers. Second, we infer parameters of an RBC relaxation model to demonstrate how Korali can improve the efficiency of hierarchical Bayesian inference problems. Lastly, we optimize the parameters for coarse-grained models for water simulation and demonstrate through a stress test the resilience of Korali’s sampling engine.

We performed all three experiments on *Piz Daint* [23], a Cray supercomputer located at the *Swiss National Supercomputing Centre (CSCS)*. We used *Piz Daint*’s GPU-based XC50 partition, comprising 5’704 compute nodes, each equipped with a single processor socket populated with a 2.6GHz 12-core (24 hardware threads) Intel Xeon E5-2690v3 “Haswell” processor and 64GB of DRAM. Each node also contains an NVIDIA “Tesla” P100 graphics processing unit (GPU) with 16GB of device memory.

4.1. Case 1: RBC Stretching Parameter Inference

RBCs are highly deformable objects, allowing for complex dynamical transitions in response to external disturbances and lay the foundation for understanding the rheology of blood in flows through capillaries, vascular networks, and medical devices. The elastic properties of RBCs, for instance, have been the point of interest of many studies due to their direct connection with pathological diseases such as malaria [24], where RBCs appear to lose their elastic abilities progressively. However, there is still significant uncertainty in the choice of the mechanical law to describe the RBC properties, as well as in the parameter values of each model [14]. To better understand such flows and simulate whole blood, we have to model the mechanics of a single RBC accurately.

In this experiment, we use a popular approach of modeling the RBC membrane as a collection of particles placed on the nodes of a triangular network [25]. The connectivity is fixed over time, and the particle positions and velocities evolve in

time according to Newton’s law. Interactions between neighboring particles are governed by a set of potential functions describing the membrane’s elastic and viscous mechanical properties. Using data for the axial and transverse extensions of RBCs under stretching [26], we infer the parameters k_s and x_0 , controlling the linear and non-linear elastic components respectively.

We used Korali to run a Bayesian inference sampling experiment using Bayesian Annealed Sequential Importance Sampling (BASIS), a reduced bias variant of the Transitional Markov Chain Monte Carlo (TMCMC) algorithm implemented in Korali. The choice of BASIS is supported by the fact that it is one of the most efficient Markov chain Monte Carlo (MCMC) algorithms in the context of Bayesian uncertainty quantification that is targeted to parallel computing architectures [27]. We configured BASIS to run a population size of 4096 samples per generation. To hold the same statistical assumptions as in the described experiment, we use a likelihood model of type Additive Normal Data. For the computational model for RBC stretching, we used MIRHEO [28], a high-performance GPU-based library for microfluidic simulations. We base our choice on the fact that MIRHEO has shown exceptionally low time to solution on several benchmark problems, outperforming current state-of-the-art packages. MIRHEO is written in C++/CUDA and targets NVIDIA GPUs. Furthermore, MIRHEO is optimized for the NVIDIA-Pascal architecture and is specifically tailored for the *Piz Daint* supercomputer platform, ensuring we get the most performance from every compute node.

4.1.1. Performance Analysis

We ran this experiment on 4096 nodes of the *Piz Daint* supercomputer, using a single worker team per node, each running a single MPI rank that uses the node’s GPU device to run an instance of MIRHEO. To evaluate the performance of this experiment, we profiled the execution of every Korali worker to determine their sampling efficiency, and show our measurements as execution timelines in Fig. 9. The horizontal axis represents the runtime, showing that one execution of the computational model ran for almost 26 minutes, spending a total of 1774 node-hours. The vertical axis represents each node, where the colored lines indicate that the node was running the computational model, and the white gaps represent segments in time where the node remained idle. The figure clearly shows that the experiment required six BASIS generations to reach convergence.

We measure the efficiency of the experiment by calculating the cumulative ratio between busy and idle times of all workers and indicate this with a black line. Since we assume that MIRHEO is already the best possible solution for our computational model, we do not factor its possible inefficiencies or overheads into the calculation, and thus consider colored lines as full node usage. As the timeline evolves, the efficiency line converges towards a steady-state value, which indicates the overall efficiency of the experiment.

Through our measurements, we have found that the sampling engine only requires a few tenths of a second to conduct computation and communication operations between gen-

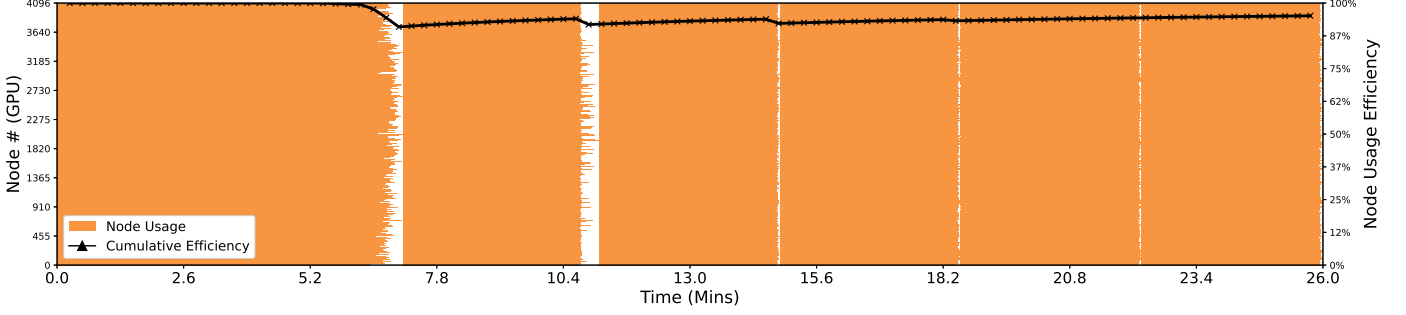


Figure 9: Core usage timelines of Korali during execution. The horizontal axis represents the elapsed time (minutes) from the start of the experiment. On the vertical axis, each line represents a different *Piz Daint* node. Whenever the line is colored, this means that MIRHEO is actively using the node’s GPU to evaluate a given sample. Blank spaces represent times where the node is idle, waiting for the next sample to be processed. The black line indicates the cumulative node usage efficiency across time, which converges to steady-state as generations are processed. A higher efficiency reflects a better node usage.

erations, and thus has a negligible impact on the total running time. In spite of Korali’s inherent performance, we have registered a sampling efficiency (\mathcal{E}) of 95.13%, meaning that there were 4.87% of wasted compute hours. The inefficiency observed is explained by the effect of load imbalance. *Load imbalance* is a phenomenon generated by the non-uniform distribution of workload among computational resources and is a common problem for parallel algorithms in general [29]. In particular, population-based methods belonging to the category of *embarrassingly parallel* [30], such as BASIS, are particularly susceptible to this phenomenon since all sample evaluations need to be synchronized before starting the next generation. Therefore, the runtime of one generation is dominated by the sample with the longest runtime.

In our previous work [31], we studied the impact of load imbalance on the BASIS algorithm, finding that some computational models show a high variance in their running time, depending on the value of their input parameters. To gain a better understanding of the effects of load imbalance (\mathcal{I}) on running time, we use the following relation:

$$\mathcal{I} = \frac{T_{max} - T_{avg}}{T_{avg}}, \quad (4)$$

where T_{max} represents the time required by the longest-running sample in a given generation, and T_{avg} represents the average running time of all samples within that generation. The value of \mathcal{I} gives an idea of how much this ratio impacts the total running time, but also how much performance could be improved had the same amount of workload be perfectly balanced. Therefore, the bigger \mathcal{I} is, the higher the impact of imbalance and the higher chances for improvement. This experiment, we observed, for each generation: $\mathcal{I} = \{0.09, 0.11, 0.02, 0.02, 0.02, 0.02\}$. Such relatively minor imbalances are explained by two redeeming factors. First, given the RBC is stretched with a constant external force, the computational parameters have little impact on the physical time – and therefore neither on simulation and computation times – it takes to reach a fully stretched state. As a consequence, BASIS starts its first generation already with small imbalances. Second, as generations are computed, and

BASIS closes in on a converged state, the variance of computational parameters is considerably reduced, thus also their running times. Fig. 9 shows that the last three generations contain little to no idle times due to imbalance. We can conclude that, for models whose parameters produce small ($\mathcal{I} < 0.1$) load imbalances, Korali provides excellent efficiency at extremely large scales.

4.2. Case 2: Red Blood Cell Membrane Dissipation

An interesting aspect of RBCs that have been observed experimentally is the effect that viscosity has on relaxation time of an RBC membrane. This phenomenon is, however, still not fully understood from a computational point of view. To gain a deeper understanding of the viscosity parameter on RBC computational models, we studied the pairwise dissipation interaction between neighboring vertices on the triangular mesh. One of the unambiguous experiments to determine the membrane viscosity is the relaxation of a stretched RBC to its equilibrium shape. Due to the presence of heterogeneous data from five different experimental studies, we formulated the inference problem for the parameter governing the dissipation interaction as a two-staged hierarchical Bayesian inference to estimate the membrane dissipation and its uncertainty, as well as reason about the validity of the RBC model implemented in MIRHEO.

In the first stage, we inferred five posterior distributions for the dissipation parameter, each conditioned on an individual data set. To infer these distributions, we defined a likelihood function comprising the execution of a virtual RBC relaxation experiment in MIRHEO that allowed us to compare simulated length scales to experimental measurements. In the second stage, we assumed that all the posterior distributions found in the first stage follow a generalized distribution that is controlled by some hyperparameters, which remained to be inferred.

We performed the sampling in stage one and two using BASIS implemented in Korali, whereas we used 512 samples in stage one, and 10000 samples in stage two. Finally, we found that the estimated membrane dissipation parameter, using maximum a posteriori (MAP), corresponds to membrane viscosity parameters estimated in the literature. The exhaustive mathematical

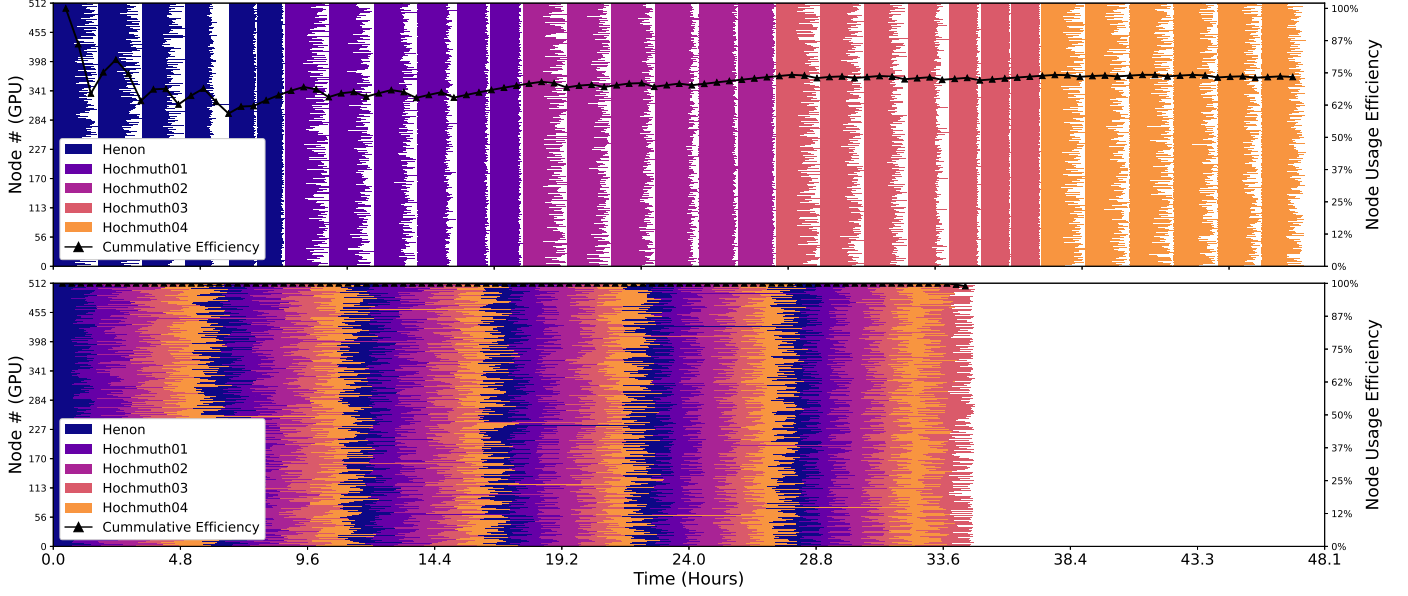


Figure 10: Core usage timelines of Korali for the five different experiment datasets, starting from Henon (darkest shade), Hochmuth01, Hochmuth02, Hochmuth03, and ending on the right with Hochmuth04 (lightest shade). On Top: Sequentially scheduled BASIS experiments, and; Bottom: Fully dynamic scheduling with Korali where samples from any experiment can be scheduled for execution on any of the available 512 nodes.

	Node #	Time (h)	Node Hours			Efficiency	Energy Usage (GJ)
			Used (Total)	Effective	Wasted		
Single Experiment	512	47.32	24227	17623	6604	72.7%	10.45
Multiple Experiments	512	34.78	17809	17623	186	98.9%	7.80

Table 1: Run statistics for the two scheduling strategies used. The energy usage measurements were obtained from *Piz Daint*’s job scheduler.

formulation of the Bayesian hierarchical model is elaborated in our previous work [31].

4.2.1. Performance Analysis

In this case study, we sample five posterior distributions of the membrane dissipation parameter (γ_C) during stage one. All five experiments share a similar setup and differ only in the initial conditions and the reference data. We ran this experiment on 512 nodes of the *Piz Daint* supercomputer, using 512 worker teams, each running a single MPI rank in its own node, with each worker running an instance of *MIRHEO*. A preliminary analysis shows that the time step of the numerical time integration scheme decreases linearly in γ_C . As a consequence, increasing values of γ_C result in an increased number of simulation steps, and thus higher execution times.

Based on the linear relationship between model run time and γ_C , and given that we sample the membrane dissipation parameter $\gamma_C \sim \mathcal{U}(8000, 32000)$ from a uniform prior distribution, we estimated a worst-case scenario for load imbalance ratio to be $I = 0.44$ with an average run time $T(\gamma_{C_{avg}}) = 1.16\text{h}$ and expected maximal runtime $T(\gamma_{C_{max}}) = 1.67\text{h}$ as $\mathbb{E}[\gamma_C] = 20000$ and $\mathbb{E}[\max \gamma_C] \approx 32000$ (in simulation units). Based upon this calculation, we can expect a sampling efficiency $\mathcal{E} = 69\%$. This estimation shows that computational resources will remain idle 31% of the time. However, such imbalance only

occurs during the first generation(s) of BASIS and is later attenuated as samples tend to concentrate around the modes of the posterior distribution.

To test whether the expected load imbalance manifested during execution, we ran each of the five BASIS sampling experiments sequentially, each within a single 512 worker node allocation. Fig. 10 (top) shows the results of our preliminary run. The run took 48.1 hours to complete on 512 nodes, requiring a total of 24.6k node hours. The figure shows the impact of load imbalance on our experiments. The black line in Fig. 10 (top) shows the time evolution of efficiency \mathcal{E} of the sequential execution. We observed a sustained efficiency of $\mathcal{E} = 72.7\%$ throughout the run, meaning that the nodes waste 27.3% of their running time. The measured load imbalance and efficiency for the preliminary runs closely follow our a priori estimations. Table 1 (row: *Single Experiment*) shows that of the 24.2k node hours consumed, only 17.6k node hours were effectively used for computation, resulting in a loss of 6.6k node hours. In total, the energy usage, as reported from *Piz Daint*’s job scheduler, was of 10.45 GJ. A direct extrapolation from the measured efficiency suggests that 2.85 GJ could have been wasted. Such misuse of computational resources motivated us to find alternative ways to reduce load imbalance.

To improve the distribution of work among nodes, we resorted to *oversubscription*, a technique that has been proposed

to improve load balancing. Exemplary applications of oversubscription in the context of parallel algorithms can be found in previous works [32, 33]. The idea of oversubscription is to subdivide the required work into more subtasks than available processors. In this way, every processor must compute on average more than one task. At any given point, if a particular processor is overloaded, one of its tasks can be bestowed to an underloaded processor. In the context of sampling, each model evaluation (sample) within a given generation can be considered as a single indivisible task. Therefore, computing as many tasks as available nodes (512, in our case) represents the case where no oversubscription is applied.

To enable our Hierarchical Bayesian experiment to benefit from oversubscription, we tried scheduling all five experiments simultaneously, such that samples from all experiments can be scheduled among any of the available nodes. This approach achieves oversubscription not by reducing the number of nodes, but by increasing the number of concurrent tasks. This approach motivated us to develop Korali’s capability to distribute the samples coming from these experiments concurrently. Fig. 10 (bottom) shows the execution of our multi-experiment approach. We observed that almost all nodes could remain busy during the entirety of execution, only to lose efficiency towards the end of the sampling process. This loss arises due to the fact that some experiments finish before others, reducing available oversubscription. The results summarized in Table 1 indicate that this strategy yields a superior efficiency (98.9%) compared to the former approach, wasting much fewer node hours (186), as well as requiring less energy (7.80 GJ). Furthermore, it also reduced the runtime from 47.2 to 34.7 hours until completion. We conclude that, for Hierarchical Bayesian studies in which computational models produce larger ($\mathcal{I} > 0.1$) load imbalances, Korali’s potential to run multiple simultaneous experiments can yield an almost perfect sampling efficiency.

4.3. Case 3: Coarse-grained models for water

Simulation of water at biologically relevant timescales remains an open research topic. In the atomistic description, each atom of the water molecule is considered as a particle, and appropriate potential functions are defined that govern the interactions among the atoms of one molecule and the interactions among molecules. The system is propagated in time using Newton’s second law. In order to accelerate the atomistic simulations, coarse-grained (CG) models of water have been proposed in the literature that map one or more molecules into one particle. Most of the mappings are based on rather ad-hoc assumptions. In [13] the authors proposed a data-driven approach, based on Bayesian model selection, for the evaluation of the CG model. The authors used experimental data of density, dielectric constant, surface tension, isothermal compressibility, and shear viscosity, and for each of the considered CG models, a Bayesian inference problem was solved.

Here, we use Korali to run the Bayesian inference experiment corresponding to the CG model, where each water molecule is mapped into one CG particle. The assumed potential between the CG particles is the Lennard-Jones potential that has two parameters. The parameters of the potential are fitted on density

experimental measurements at a specified temperature. To hold the same statistical assumptions as in the described experiment, we use a likelihood model of type `Multiplicative Normal Data`. We then found the parameters that maximize the posterior distribution using CMA-ES with a population size of 16 samples per generation. For the computational model, we used LAMMPS (Large-scale Atomic/Molecular Massively Parallel Simulator) [34], a well-known molecular dynamics simulation library that models atoms or ensembles of particles in solid, liquid or gaseous state.

4.3.1. Resilience Analysis

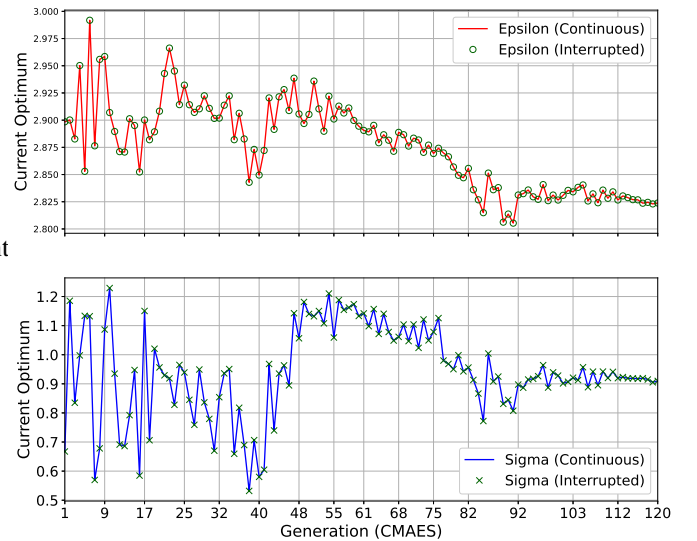


Figure 11: Evolution of the (best) parameter values that maximize the posterior distribution of the Bayesian problem comparing, in solid lines, the experiment in which all generations of CMA-ES ran uninterrupted and, in markers, the experiment which has interrupted every 15 minutes. Vertical lines indicate the generations at which the interrupted experiment was restarted. The figure shows a perfect overlap between solid lines and markers, showing that both experiments traversed the same evolution and final results.

We ran this experiment on 16 nodes of the *Piz Daint* supercomputer, using two workers for each node. Each worker ran an instance of LAMMPS using 2 MPI ranks and 12 cores per rank for full usage of the node’s 24 hardware threads (the model does not employ GPU resources). Since it would have been difficult to modify LAMMPS to link it directly with the sampling engine, we used Korali’s support for external models, requiring only LAMMPS-specific file-based parameter write, execution, and result gathering interfaces.

We used this experiment to show that Korali can provide resilient checkpoint-based fault tolerance, even for out-of-the-box libraries such as LAMMPS. To evaluate this feature, we ran the same experiment with the same random seed twice. In the first run, we ran the experiment to completion as a single job and without interruptions. In the second run, we configured the job scheduler to run for only 15 minutes at a time, after which the execution would be forcibly terminated by the system. As a result, the execution of CMA-ES would be interrupted every 7~8

generations, crashing abruptly upon timeout. To complete the experiment, we automatized the scheduling of jobs to be dispatched after the previous' cancellation, reloading the internal state of CMA-ES every time it was restarted.

Fig. 11 shows the comparison between the per generation evolution of parameter optima between the single-run execution (continuous line), and the interrupted execution (markers) for both of the experiment's parameters. In the figure, vertical grid lines indicate the generation at which the interruptions occurred for the latter, for a total of 16 experiments. The figure indicates that the final results produced were equal and that they followed the same convergence path. These results prove that, even through repeated system failures, Korali suffers no detrimental effects on correctness.

5. Related Work

Many of the problems and solver methods currently implemented in Korali can also be recognized across various other statistical UQ software. The most prominent and extensive tools are *ABC-SysBio* [3], *APT-MCMC* [4, 35], *BCM* [36, 37], *BioBayes* [38], *$\Pi 4U$* [8], *MUQ* [39], *PSUADE* [5], *QUESO* [6], *Scanner-Bit* [40] (a *GAMBIT* [41, 42] module), which are standalone applications; *Chaospy* [43], *Uncertainpy* [44, 45], *UQPy* [46], which are publicly available Python packages; *Stan* [7], a programming language for statistical inference; and *UQLab* [2], a MATLAB framework. Some of the previously mentioned software (e.g., *Stan*, *UQLab* and *UQPy*) are very rich in the number of available solver and problem types, but have grown over the years in a way such that they lack flexibility and scalability. In addition, some tools explicitly target specific research domains, such as *ABC-SysBio* and *BioBayes* for biology and *ScannerBit* for astrophysics, and hence do not compare with Korali which is designed for general scientific applications. On the other hand, we expect Korali's capabilities to grow based on demand, driven by the needs of the scientific community, thanks to its modular design and purely descriptive interface.

Of the aforementioned tools, few offer scalable evaluation of computationally demanding models. *APT-MCMC* and *BCM* offers thread-level parallel algorithms, while *PSUADE*, *QUESO*, *Scanner-Bit*, and *UncertainPy* offer process-level parallelism. Although these approaches are effective in harnessing the computational power of multi-core processors, they were not extended to distributed systems. On the other hand, the *EasyVVUQ* [9] (part of the *VECMAtk* project [47]), *Dakota* [10], and *$\Pi 4U$* [8] frameworks offer different degrees of support for optimization and UQ at larger scales.

EasyVVUQ is a python-based library for designing UQ workflows that can run over *FabSim3* [48], a scheduler for the execution of such workflows. The latest reported results from this framework show experimental results on a variety of experiments, including the uncertainty propagation of the parameters of a thermonuclear fusion model, using up to 512 CPU-hours [47]. Although these results show some promise for larger-scale support in the future, they are still two orders of magnitude below the demands of the applications we have modeled in this work.

Dakota is a C++-based framework for uncertainty quantification, which can interface with simulation software packages through a multi-level parallelism interface. Like Korali, DAKOTA's distributed engine uses the Message Passing Interface (MPI) and a fork/join strategy for concurrent execution of out-of-the-box software. We have not found published results for Dakota-enabled experiments that reach the at-scale results shown in this paper.

Finally, the *$\Pi 4U$* library has shown promising results on large-scale evaluations of Bayesian inference experiments. Nevertheless, Korali's scheduling approach has shown to decrease imbalance even further as it can run multiple concurrent experiments shared among a shared pool of computational resources. Finally, none of the modularity, fault-tolerance, and reproducibility features present in Korali are currently offered by *$\Pi 4U$* .

6. Conclusions

We have presented Korali, a novel framework for the efficient deployment of stochastic computational models in parallel computing architectures. The software introduces mechanisms to enable a scalable, fault-tolerant, and reproducible execution of experiments from a wide range of problem types and solver methods. The software has an extensible design and intuitive interface to automate the deployment of stochastic methods at large scales.

Our experimental results have shown that Korali is capable of attaining high sampling efficiencies on up to 4096 nodes of *Piz Daint*, which corresponds to 71% of the entire supercomputer. Furthermore, we have shown that many experiments can be executed simultaneously in the context of hierarchical Bayesian on a common set of computational resources. The present approach minimizes load imbalance and achieves almost perfect node usage, even when the computational models show a high parameter-based runtime variance. Finally, we have shown that the software can run out-of-the-box libraries, such as LAMMPS, without the need for refactoring, and providing resilient fault-tolerance mechanisms.

6.1. Future Work

We are currently considering algorithmic developments for CMA-ES and BASIS variants that would allow to partially advance to the next generation as soon as a certain information threshold is met. In this way, a new set of samples can start to be evaluated while waiting for the ones in the previous generation.

We are also integrating machine learning and Reinforcement Learning (RL) methods, such as *V-RACER* [49] into the Korali framework. These RL methods benefit from highly distributed implementations [50] and target the optimization of a policy for an agent acting in an environment to collect rewards. We believe that a platform integrating machine learning, stochastic optimization, and uncertainty quantification will be of great value for the broad scientific community.

Acknowledgements

We would like to thank L. Amoudruz, A. Economides, I. Kicic, P. Weber, and F. Wermelinger for providing us with their support and invaluable feedback on the writing of this article. We acknowledge support by the European Research Council (ERC Advanced Grant 341117) and computational resources granted by the Swiss National Supercomputing Center (CSCS) under project ID s929.

References

- [1] S. Ashby, P. Beckman, J. Chen, P. Colella, B. Collins, D. Crawford, J. Dongarra, D. Kothe, R. Lusk, P. Messina, et al., The opportunities and challenges of exascale computing, Summary Report of the Advanced Scientific Computing Advisory Committee (ASCAC) Subcommittee (2010) 1–77.
- [2] UQLab, <https://www.uqlab.com>, accessed: 2019-06-13.
- [3] J. Liepe, C. Barnes, E. Cule, K. Erguler, P. Kirk, T. Toni, M. P. Stumpf, ABC-SysBioapproximate Bayesian computation in Python with GPU support, *Bioinformatics* 26 (14) (2010) 1797–1799. doi:10.1093/bioinformatics/btq278.
- [4] L. A. Zhang, A. Urbano, G. Clermont, D. Swigon, I. Banerjee, R. S. Parker, Apt-mcmc, a c++/python implementation of markov chain monte carlo for parameter identification, *Computers & Chemical Engineering* 110 (2018) 1–12. doi:<https://doi.org/10.1016/j.compchemeng.2017.11.011>.
- [5] PSUADE, <https://computation.llnl.gov/projects/psuade-uncertainty-quantification>, accessed: 2019-06-13.
- [6] E. E. Prudencio, K. W. Schulz, The parallel c++ statistical library ‘queso’: Quantification of uncertainty for estimation, simulation and optimization, in: M. Alexander, P. D’Ambra, A. Belloum, G. Bosilca, M. Cannataro, M. Danelutto, B. Di Martino, M. Gerndt, E. Jeannot, R. Namyst, J. Roman, S. L. Scott, J. L. Traff, G. Vallée, J. Weidendorfer (Eds.), *Euro-Par 2011: Parallel Processing Workshops*, Springer Berlin Heidelberg, Berlin, Heidelberg, 2012, pp. 398–407.
- [7] Stan, <https://mc-stan.org>, accessed: 2019-06-13.
- [8] P. Hadjidoukas, P. Angelikopoulos, C. Papadimitriou, P. Koumoutsakos, Π4U: A high performance computing framework for Bayesian uncertainty quantification of complex models, *Journal of Computational Physics* 284 (2015) 1–21. doi:10.1016/j.jcp.2014.12.006.
- [9] EasyVVUQ, <https://easyvvuq.readthedocs.io/en/latest/>, accessed: 2019-06-13.
- [10] B. M. Adams, W. Bohnhoff, K. Dalbey, J. Eddy, M. Eldred, D. Gay, K. Haskell, P. D. Hough, L. P. Swiler, Dakota, a multilevel parallel object-oriented framework for design optimization, parameter estimation, uncertainty quantification, and sensitivity analysis, 2009.
- [11] J. Dongarra, P. Beckman, T. Moore, P. Aerts, G. Aloisio, J.-C. Andre, et al., The International Exascale Software Project Roadmap, *Int. J. High Perform. Comput. Appl.* 25 (1) (2011) 3–60. doi:10.1177/1094342010391989.
- [12] T. M. Fischer, R. Korzeniewski, Threshold shear stress for the transition between tumbling and tank-treading of red blood cells in shear flow: dependence on the viscosity of the suspending medium, *Journal of Fluid Mechanics* 736 (2013) 351365. doi:10.1017/jfm.2013.496.
- [13] J. Zavadlav, G. Arampatzis, P. Koumoutsakos, Bayesian selection for coarse-grained models of liquid water, *Scientific Reports* 9 (1) (2019) 1–10. doi:10.1038/s41598-018-37471-0.
- [14] J. Sigüenza, S. Mendez, F. Nicoud, How should the optical tweezers experiment be used to characterize the red blood cell membrane mechanics?, *Biomechanics and modeling in mechanobiology* 16 (5) (2017) 1645–1657.
- [15] N. Hansen, S. D. Muller, P. Koumoutsakos, Reducing the Time Complexity of the Derandomized Evolution Strategy with Covariance Matrix Adaptation (CMA-ES) Nikolaus, *Evolutionary Computation* 11 (1) (2003) 1–18.
- [16] S. Wu, P. Angelikopoulos, C. Papadimitriou, P. Koumoutsakos, Bayesian Annealed Sequential Importance Sampling (BASIS): an unbiased version of Transitional Markov Chain Monte Carlo, *ASCE-ASME Journal of Risk and Uncertainty in Engineering Systems, Part B: Mechanical Engineering* 4 (1) (2018) 011008.
- [17] J. Ching, Y.-c. Chen, Transitional Markov Chain Monte Carlo Method for Bayesian Model Updating, Model Class Selection, and Model Averaging, *Journal of Engineering Mechanics* 133 (7) (2007) 816–832.
- [18] MPI Forum, <https://www.mpi-forum.org/>.
- [19] J. Bachan, S. B. Baden, S. Hofmeyr, M. Jacquelin, A. Kamil, D. Bonachea, P. H. Hargrove, H. Ahmed, Upc++: A high-performance communication framework for asynchronous computation, in: 2019 IEEE International Parallel and Distributed Processing Symposium (IPDPS), IEEE, 2019, pp. 963–973.
- [20] T. Bray, et al., The javascript object notation (json) data interchange format, <http://www.rfc-editor.org>.
- [21] reStructuredText Markup Specification, <https://docutils.sourceforge.io/docs/ref/rst/restructuredtext.html>, accessed: 2020-03-26.
- [22] Koral User Manual, <https://www.cse-lab.ethz.ch/koral/docs/>, accessed: 2020-03-26.
- [23] CSCS piz daint, <https://www.cscs.ch/computers/piz-daint/>, accessed: 30-10-2019.
- [24] S. Suresh, J. Spatz, J. P. Mills, A. Micoulet, M. Dao, C. T. Lim, M. Beil, T. Seufferlein, Connections between single-cell biomechanics and human disease states: Gastrointestinal cancer and malaria, *Acta Biomaterialia* 1 (1) (2005) 15–30. doi:10.1016/j.actbio.2015.07.015.
- [25] D. A. Fedosov, B. Caswell, G. E. Karniadakis, A Multiscale Red Blood Cell Model with Accurate Mechanics, Rheology, and Dynamics, *Biophysical Journal* 98 (10) (2010) 2215–2225.
- [26] J. P. Mills, L. Qie, M. Dao, C. T. Lim, S. Suresh, Nonlinear Elastic and Viscoelastic Deformation of the Human Red Blood Cell with Optical Tweezers, *MCB Tech Science Press* 1 (3) (2004) 169–180.
- [27] S. Wu, P. Angelikopoulos, G. Tauriello, C. Papadimitriou, P. Koumoutsakos, Fusing heterogeneous data for the calibration of molecular dynamics force fields using hierarchical Bayesian models, *The Journal of Chemical Physics* 145 (24).
- [28] D. Alexeev, L. Amoudruz, S. Litvinov, P. Koumoutsakos, Mirheo: High-performance mesoscale simulations for microfluidics (2020). doi:10.1016/j.cpc.2020.107298.
- [29] R. K. Brunner, L. V. Kalé, Handling application-induced load imbalance using parallel objects, *Parallel and Distributed Computing for Symbolic and Irregular Applications* (2000) 167–181.
- [30] K. Asanovic, R. Bodik, B. C. Catanzaro, J. J. Gebis, P. Husbands, K. Keutzer, D. A. Patterson, W. L. Plishker, J. Shalf, S. W. Williams, et al., The landscape of parallel computing research: A view from Berkeley, Tech. rep., Technical Report UCB/EECS-2006-183, EECS Department, University of (2006).
- [31] D. Wälchli, S. M. Martin, A. Economides, L. Amoudruz, G. Arampatzis, X. Bian, P. Koumoutsakos, Load Balancing in Large Scale Bayesian Inference, in: *Proceedings of the The Platform for Advanced Scientific Computing (PASC) Conference 2020*, to appear, 2020, pp. 0–0.
- [32] S. Bak, H. Menon, S. White, M. Diener, L. V. Kalé, Multi-Level Load Balancing with an Integrated Runtime Approach, in: 18th IEEE/ACM International Symposium on Cluster, Cloud and Grid Computing, CCGRID 2018, Washington, DC, USA, May 1-4, 2018, 2018, pp. 31–40.
- [33] S. M. Martin, MATE, a Unified Model for Communication-Tolerant Scientific Applications, Ph.D. thesis, University of California, San Diego (2018).
- [34] S. Plimpton, Fast Parallel Algorithms for Short Range Molecular Dynamics, *Journal of Computational Physics* 117 (June 1994) (1995) 1–19. doi:10.1006/jcph.1995.1039. URL <http://lammmps.sandia.gov>
- [35] APT-MCMC, <https://apt-mcmc.readthedocs.io/en/latest/>, accessed: 2020-02-27.
- [36] B. Thijssen, T. M. H. Dijkstra, T. Heskes, L. F. A. Wessels, Bcm: toolkit for bayesian analysis of computational models using samplers, *BMC Systems Biology* 10 (1) (2016) 100. doi:10.1186/s12918-016-0339-3. URL <https://doi.org/10.1186/s12918-016-0339-3>
- [37] BCM, <http://ccb.nki.nl/software/bcm/>, accessed: 2019-06-14.
- [38] V. Vyshemirsky, M. Girolami, BioBayes: A software package for Bayesian inference in systems biology, *Bioinformatics* 24 (17) (2008) 1933–1934. doi:10.1093/bioinformatics/btn338.
- [39] MUQ - MIT Uncertainty Quantification Library, <http://muq.mit.edu>,

- accessed: 2020-02-27.
- [40] G. D. Martinez, J. McKay, B. Farmer, P. Scott, E. Roebber, A. Putze, J. Conrad, Comparison of statistical sampling methods with scannerbit, the gambit scanning module, *The European Physical Journal C* 77 (11). doi:10.1140/epjc/s10052-017-5274-y. URL <http://dx.doi.org/10.1140/epjc/s10052-017-5274-y>
 - [41] The GAMBIT Collaboration, Gambit: the global and modular beyond-the-standard-model inference tool, *The European Physical Journal C* 77 (11) (2017) 784. doi:10.1140/epjc/s10052-017-5321-8.
 - [42] GAMBIT, <https://gambit.hepforge.org>, accessed: 2019-06-13.
 - [43] chaospy, <https://chaospy.readthedocs.io/en/master/tutorial.html>, accessed: 2020-02-28.
 - [44] S. Tennøe, G. Halnes, G. T. Einevoll, Uncertainpy: A python toolbox for uncertainty quantification and sensitivity analysis in computational neuroscience, *Frontiers in Neuroinformatics* 12 (2018) 49. doi:10.3389/fninf.2018.00049.
 - [45] Uncertainpy, <https://uncertainpy.readthedocs.io>, accessed: 2019-06-13.
 - [46] UQpy, <https://github.com/SURGroup/UQpy>, accessed: 2019-06-13.
 - [47] D. Groen, R. A. Richardson, D. W. Wright, V. Jancauskas, R. Sinclair, P. Karlshoefer, M. Vassaux, H. Arabnejad, T. Piontek, P. Kopta, et al., Introducing vecmatk-verification, validation and uncertainty quantification for multiscale and hpc simulations, in: *International Conference on Computational Science*, Springer, 2019, pp. 479–492.
 - [48] D. Groen, A. P. Bhati, J. Suter, J. Hetherington, S. J. Zasada, P. V. Coveney, Fabsim: Facilitating computational research through automation on large-scale and distributed e-infrastructures, *Computer Physics Communications* 207 (2016) 375 – 385. doi:<https://doi.org/10.1016/j.cpc.2016.05.020>.
 - [49] G. Novati, P. Koumoutsakos, Remember and forget for experience replay, in: *Proceedings of the 36th International Conference on Machine Learning*, 2019. URL <http://www.cse-lab.ethz.ch/wp-content/papercite-data/pdf/novati2019a.pdf>
 - [50] L. Espeholt, H. Soyer, R. Munos, K. Simonyan, V. Mnih, T. Ward, Y. Doron, V. Firoiu, T. Harley, I. Dunning, S. Legg, K. Kavukcuoglu, Impala: Scalable distributed deep-rl with importance weighted actor-learner architectures (2018). [arXiv:1802.01561](https://arxiv.org/abs/1802.01561).